Hyperechoes

Juergen Hennig* and Klaus Scheffler

A novel spin-echo-based refocusing strategy called a hyperecho mechanism is introduced by which the full coherence of magnetization submitted to a sequence of arbitrary RF pulses can be reinstalled. First implementations illustrate the potential of hyperecho formation—especially for Rapid Acquisition with Relaxation Enhancement (RARE) imaging, in which the full image intensity can be retrieved using a fraction of the RF power of a fully refocused sequence. The contribution of stimulated echo pathways to the hyperecho signal leads to an increased signal intensity at a given refocusing time for tissues with $T_1 > T_2$. For identical T_2 contrast, longer echo times have to be used. Further possibilities for using hyperechoes in gradient-echo sequences and for spin selection are discussed. Magn Reson Med 46:6–12, 2001. © 2001 Wiley-Liss, Inc.

Key words: hyperecho; spin echo; RARE; DEFT

The spin-echo mechanism, first described in 1950 (1), has turned out to be extremely useful for MR tomography. Its inherent ability to refocus local field inhomogeneities and susceptibility effects, and its rather straightforward contrast behavior are the basis of the extremely widespread use of spin-echo-based sequences in routine imaging. Rapid Acquisition with Relaxation Enhancement (RARE) (or turbo spin echo, fast spin echo. . .) sequences (2) use a Carr-Purcell-Meiboom-Gill (CPMG) multiecho train (3) to acquire images within reasonable acquisition times while maintaining the beneficial signal behavior of spin-echo formation. As a consequence of the constructive superposition of multiple refocusing pathways, CPMG sequences deliver high signal amplitudes even for low refocusing flip angles, which can be even further improved using nonconstant flip angles at least over the first few echoes (4–7). This is especially useful in high-field applications in which specific absorption rate (SAR) problems prohibit the use of long trains of 180° pulses.

The application of multiple refocusing pulses with small flip angles will in general lead to a more and more complex distribution of the isochromats in the rotating frame. After only a few refocusing pulses, the magnetization vectors will appear to be hopelessly scrambled. Even in CPMG sequences, the best one can hope for is to reduce the apparently inevitable signal loss caused by the incoherent superposition of the isochromats. The purpose of this study was to demonstrate simply how magnetization scrambled by any arbitrary multipulse sequence can be unwound and a spin echo with full intensity can be formed. After introduction of the basic principles, a few examples of sequences in which this hyperecho mechanism appears to be useful are demonstrated.

Department of Diagnostic Radiology, Section of Medical Physics, Freiburg, Germany.

*Correspondence to: Juergen Hennig, Dept. of Diagnostic Radiology, Section of Medical Physics, Hugstetterstr. 55, 79106 Freiburg, Germany. E-mail: hennig@nz11.ukl.uni-freiburg.de

Received 14 December 2000; revised 23 February 2001; accepted 28 February 2001.

THEORY

The hyperecho mechanism is based on simple symmetry relations of vector rotation in space (illustrated in Fig. 1). The first such relation (Fig. 1a) can be stated as: rotation $\mathrm{Rot}_z(\varphi)$ of a vector $\mathbf{V}(x,y,z)$ around the z-axis by a rotation angle φ followed by rotation $\mathrm{Rot}_y(180°)$ around the y-axis by 180° followed by another rotation around z with φ is equivalent to direct rotation of $\mathbf{V}$ around y by 180°:

$$\mathrm{Rot}_z(\varphi)\mathrm{Rot}_y(180°)\mathrm{Rot}_z(\varphi)\mathbf{V}(x,\,y,\,z) = \mathrm{Rot}_y(180°)\mathbf{V}(x,\,y,\,z). \quad [1]$$

The second symmetry relation (illustrated in Fig. 1b) is a consequence of the rather trivial fact that the rotation angle is additive for subsequent rotations around one axis:

$$\mathrm{Rot}_y(-\alpha)\mathrm{Rot}_y(180°)\mathrm{Rot}_y(\alpha)\mathbf{V}(x,\,y,\,z) = \mathrm{Rot}_y(180°)\mathbf{V}(x,\,y,\,z). \quad [2]$$

Bearing in mind that rotation $\mathrm{Rot}_\phi(\alpha)$ around an axis that lies in the x-y plane at an angle ϕ from the y-axis is equivalent to:

$$\mathrm{Rot}_\phi(\alpha)\mathbf{V}(x,\,y,\,z) = \mathrm{Rot}_z(\phi)\mathrm{Rot}_y(\alpha)\mathrm{Rot}_z(-\phi)\mathbf{V}(x,\,y,\,z) \quad [3]$$

a third symmetry condition (Fig. 1c) can be derived from Eqs. [1]–[3], which can be stated as:

$$\mathrm{Rot}_{-\phi}(-\alpha)\mathrm{Rot}_y(180°)\mathrm{Rot}_\phi(\alpha)\mathbf{V}(x,\,y,\,z) = \mathrm{Rot}_y(180°)\mathbf{V}(x,\,y,\,z). \quad [4]$$

More complex sequences of rotations, which are all identical to $\mathrm{Rot}_y(180°)$ $\mathbf{V}(x,y,z)$, can be derived from combining Eqs. [1] and [4]:

$$\mathrm{Rot}_{-\phi}(-\alpha)\mathrm{Rot}_z(\varphi)\mathrm{Rot}_y(180°)\mathrm{Rot}_z(\varphi)\mathrm{Rot}_\phi(\alpha)\mathbf{V}(x,\,y,\,z) = \mathrm{Rot}_y(180°)\mathbf{V}(x,\,y,\,z) \quad [5]$$

or in general

$$\mathrm{Rot}_{-\phi n}(-\alpha_n)\mathrm{Rot}_z(\varphi_n)\ldots\mathrm{Rot}_{-\phi 1}(-\alpha_1)\mathrm{Rot}_z(\varphi_1)\mathrm{Rot}_y(180°) \times \mathrm{Rot}_z(\varphi_1)\mathrm{Rot}_{\phi 1}(\alpha_1)\ldots\mathrm{Rot}_z(\varphi_n)\mathrm{Rot}_\phi(\alpha_n)*\mathbf{V}(x,\,y,\,z) = \mathrm{Rot}_y(180°)*\mathbf{V}(x,\,y,\,z). \quad [6]$$

These as yet strictly geometric relations of vector rotation can be easily transformed into MR pulse sequences by observing that vector rotation of magnetization $\mathbf{M}$ (Mx, My, Mz) around a tilted axis in the transverse plane corresponds to application of an RF pulse $P(\alpha, \phi)$ with flip angle α and phase ϕ. Rotation around z corresponds to a phase evolution $\varphi(o, t)$ of $\mathbf{M}$ in between pulses. $\varphi(o, t)$ describes

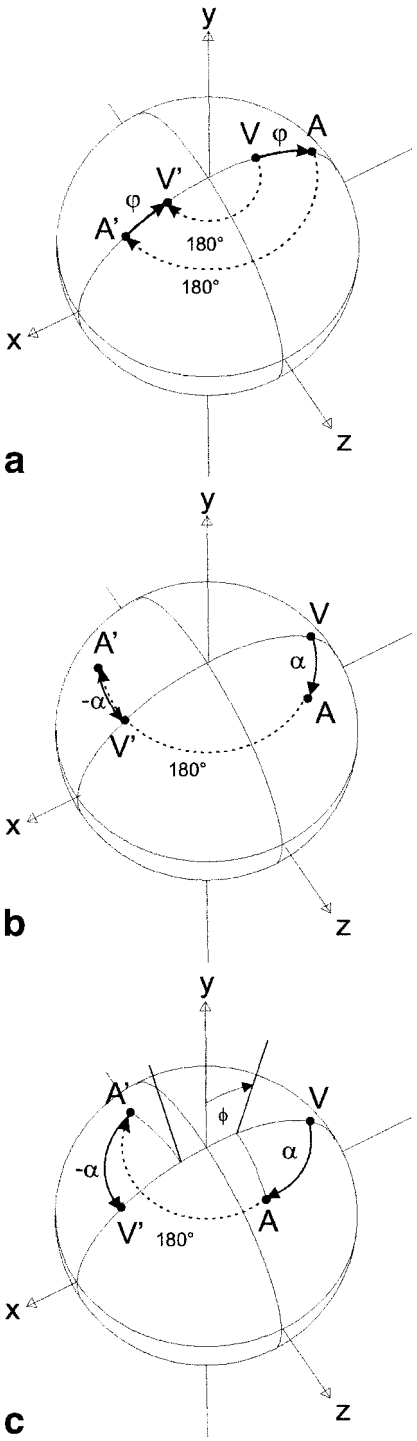

FIG. 1. Graphical demonstration of equivalent vector operations. **a:** Rotation of vector **V** represented by its endpoint as a dot on the sphere around the z-axis by an angle φ to **A** followed by a 180° rotation around the y-axis (orthogonal to the plane of the graph) to **A′** followed by another rotation around z with φ leads to **V′**, which is equivalent to a direct 180° rotation of **V** around y. **b:** Rotation of **V** around the y-axis by an angle α followed by a 180° rotation around the y-axis, followed by a rotation around y with $-\alpha$, which is equivalent to a direct 180° rotation of **V** around y. **c:** The equivalent relationship described in Eq. [4] for rotations around an axis that is tilted in the x-y plane with respect to the y-axis by an angle ϕ.

the total dephasing between pulses, which will depend in part on the effect of magnetic field gradients.

Equation [1] then corresponds to classical spin-echo formation and states that refocusing will occur irrespective of the dephasing φ between pulses. Equation [6] can now be used to build pulse sequences with $N = 2n + 1$ pulses, which are symmetrical around a central 180° pulse $P(\alpha_{n+1}, \phi_{n+1}) = P(180°, 0)$ according to the following conditions for the RF pulses $P_i(\alpha_i, \phi_i)$ and interpulse dephasings φ_i (ω_i, t_i):

$$P_i(\alpha_i, \phi_i) = P_i(-\alpha_{N+1-i}, -\phi_{N+1-i}) = P_i(\alpha_{N+1-i}, 180°-\phi_{N+1-i}) \quad [7]$$

and

$$\varphi_i(\omega_i, t_i) = \varphi_i(\omega_{N-i}, t_{N-i}). \quad [8]$$

Such a pulse sequence is shown in Fig. 2a. According to Eqs. [1]–[6] this pulse sequence will act like a single 180° pulse irrespective of the choice of α_i, ϕ_i, φ_i. If this sequence is preceded by a 90° excitation pulse (Fig. 2b), the pulses will act as refocusing pulses, and the resulting signal can be regarded as an echo of echoes, which leads to the term "hyperecho." Although in general one might only be interested in the echo amplitudes, Eqs. [1]–[6] apply to all signal time points in between pulses. If the signal is represented in complex notation, where the real part is aligned in parallel to the phase φ_0 of the central 180° pulse, it can be seen from Eq. [6] that the signal in corresponding mirror-symmetrical time intervals will be time-reversed complex conjugates of each other. Of course, all of these considerations apply only if relaxation effects are neglected.

The most simple hyperecho sequence is a 90°(excitation)-α-180°-$(-\alpha)$ triple echo sequence. In this case, it is still feasible to use an analytical calculation of the signal intensity following the different refocusing pathways: If the signal amplitude after the excitation pulse is labeled as I_0, and if the phase of the excitation pulse is orthogonal to that of the following three pulses, the intensity I_{st} of the stimulated echo will be given by $I_{st} = I_0\ 1/2\ \sin^2(\alpha)$. The second signal to consider corresponds to the triple refocused spin echo, the intensity of which will be $I_{3e} = I_0\ \sin^2(\alpha/2)\ \sin^2(-\alpha/2) = I_0\ \sin^4(\alpha/2)$. Finally, a spin echo will be formed by transverse magnetization, which escapes both the α and $-\alpha$ pulse, but is refocused by the central 180° pulse. Its intensity will be $I_{1e} = I_0 \cos^4(\alpha/2)$. The total intensity I_{he} of the hyperecho will thus be

$$I_{he} = I_0(1/2 \sin^2(\alpha) + \sin^4(\alpha/2) + \cos^4(\alpha/2)). \quad [9]$$

With $\sin(\alpha) = 2\ I_0 \sin(\alpha/2) \cos(\alpha/2)$ this leads to $I_{he} = I_0$ independent of α.

This simple example also shows that the relaxation behavior of a hyperecho experiment will depend on both T_1 and T_2 due to the contribution of stimulated echo pathways. For tissues with $T_1 > T_2$ the intensity of the hyperecho will then depend on the actual flip angles and phases used. This is illustrated in Fig. 3, which shows the hyperecho intensities for a hyperecho sequence with 2n +

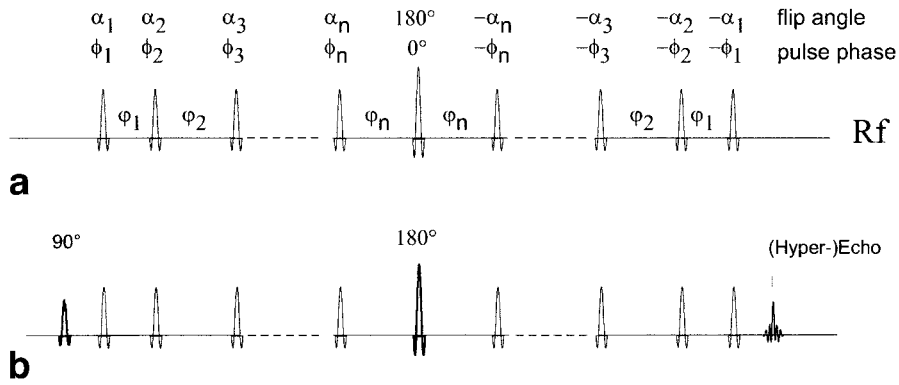

FIG. 2. **a:** Illustration of a hyperecho sequence according to Eqs. [5] and [6]. Any sequence of pulses following the shown symmetry will act like a single 180° pulse as long as relaxation effects are ignored. **b:** If preceded by a 90° excitation pulse, it will lead to the formation of a hyperecho.

1 equally spaced refocusing pulses described by 90°(excitation)-$(\alpha)_n$-180°-$(-\alpha)_n$ as a function of α and 2n + 1. The interecho interval has been adjusted to 80 ms/(2n + 1) such that the hyperecho always occurs at TE = 80 ms, T_2 = 50 ms, and T_1 = 800 ms, which roughly corresponds to the gray matter of brain. T_2 was assumed to be independent of the interecho interval and diffusion effects have been neglected. It is clear that for α = 0 (single spin echo) and α = 180° (CPMG multiecho) the hyperecho intensity will solely depend on T_2. For intermediate α, the signal decay will be more or less dependent on T_1. The second vertical scale to the right of Fig. 3 represents δt(Mz) defined as the proportionate amount of TE, during which the magnetization evolves as z-magnetization. δt(Mz) = 1/3 represents an isotropic distribution of the Mx, My, and Mz components. Apparently for large n this case is approached for α ~ 60°. For small n and an appropriate choice of α, the stimulated echo pathways will dominate leading to even higher intensities. As a somewhat surprising consequence from these considerations, it can be concluded that the signal intensity of a hyperecho experiment can be even higher than that achieved in a fully refocused CPMG experiment. For biological tissues with $T_1 \gg T_2$ the T_1 effect on the hyperecho intensity can be neglected for the moderate TEs commonly used in T_2-weighted experiments. It then follows that a nearly identical T_2 contrast compared to a conventional multiecho experiment with an effective TE (TE_{eff}) will be achieved at $TE_{he} = 1/(1 - \delta t(Mz))\ TE_{eff}$. For δt(Mz) = 1/3, this will lead to a prolongation of TE_{eff} by 50% in order to achieve comparable T_2 contrast.

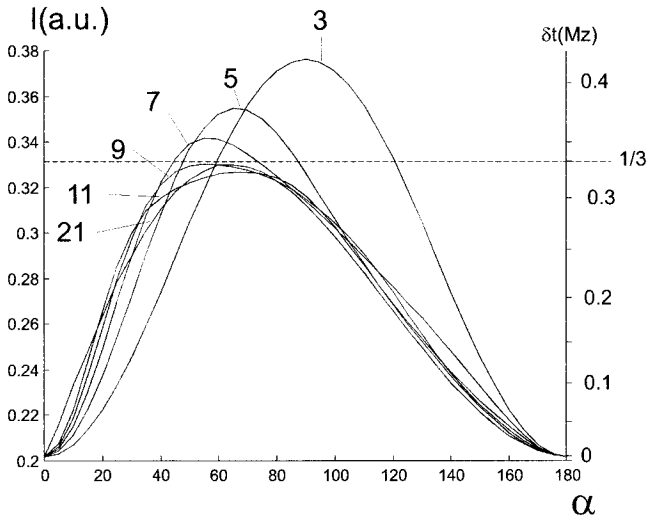

FIG. 3. Signal intensities I of the hyperecho at TE = 80 ms for tissue, with T_2 = 50 ms and T_1 = 800 ms for hyperecho trains with equally spaced refocusing pulses as a function of the refocusing flip angle α for different numbers of refocusing pulses. The vertical scale on the right represents δt(Mz), the fractional contribution of stimulated echo pathways to the hyperecho signal formation.

HYPERECHOES IN RARE SEQUENCES

Optimized Amplitudes Along the Echo Train at Reduced SAR

The most straightforward practical application of hyperechoes is their introduction into a RARE experiment to maximize one or several signals within the echo train. According to the contrast behavior of RARE, in which the contrast has been shown to be determined by the echoes with zero phase encoding, it appears to be particularly attractive to refocus this particular signal via the hyperecho mechanism. If the phase-encoding scheme is applied such that this echo occurs at the (2n + 1) echo, then the central refocusing pulse for hyperecho formation has to be placed before the (n + 1) refocusing period. Since the hyperecho mechanism will time-reverse all echoes, it will lead to a return of the initial signal modulations over the first few echoes, which is inherent to echo trains with low and constant refocusing flip angles. To avoid image artifacts it is therefore advisable to use variable flip angles leading to smooth echo amplitudes for this particular implementation (5,6). Even a simple first refocusing pulse with flip angle 90° + α/2 will produce satisfactory results (7) at least as long as α is not too small. For multicontrast implementations, in which images with different contrasts are to be acquired by echo sharing, multiple hyperechoes at the appropriate TEs can be performed.

Hyperecho Driven Equilibrium Fourier Transform (DEFT)

Another range of applications in which the hyperecho mechanism promises to be of practical use is in DEFT sequences. The principle of bringing transverse magnetization back to the z-axis for shortening the time necessary for signal recovery has been previously suggested for imaging (8) and has been revisited recently for RARE sequences (9). Busse et al. (9) showed that the penalty for

using low refocusing flip angles in DEFT sequences is quite severe, since both the steady-state intensity and the signal generated therefrom will be attenuated. Low flip angles will be especially required at higher fields, in which T_1 relaxation times are also long, and therefore DEFT-type sequences appear to be especially beneficial.

By using RARE with refocusing pulses according to Eqs. [5] and [6], such that the hyperecho occurs at the time of the final flipback pulse, the full magnetization can be retrieved and brought back to the z-axis. The resulting hyperecho RARE sequence will consequently suffer the same mild signal loss from the reduced refocusing flip angle as found in conventional RARE sequences. In particular, it should be pointed out that for tissues with $T_1 = T_2 \gg$ TR and TR equal to the length of the echo train, DEFT will produce 50% of the equilibrium signal at a fraction of the total acquisition time. It should also be noted that under these conditions a variation of the length of the echo train and a concordant variation of TR will change the T_1 and T_2 contrasts of the images without changing the total acquisition time.

For implementation, the whole sequence (including the initial excitation pulse) can be incorporated according to Eqs. [5] and [6], which will lead to magnetization aligned along the z-axis, which can be inverted using a proper (preferably adiabatic) inversion pulse. Alternatively, alignment along z can be achieved by a terminal $-90°$ flipback pulse. Of course, the use of hyperechoes for optimizing the driven equilibrium can be combined with the previously described application of hyperechoes to maximize the zero phase-encoding signal.

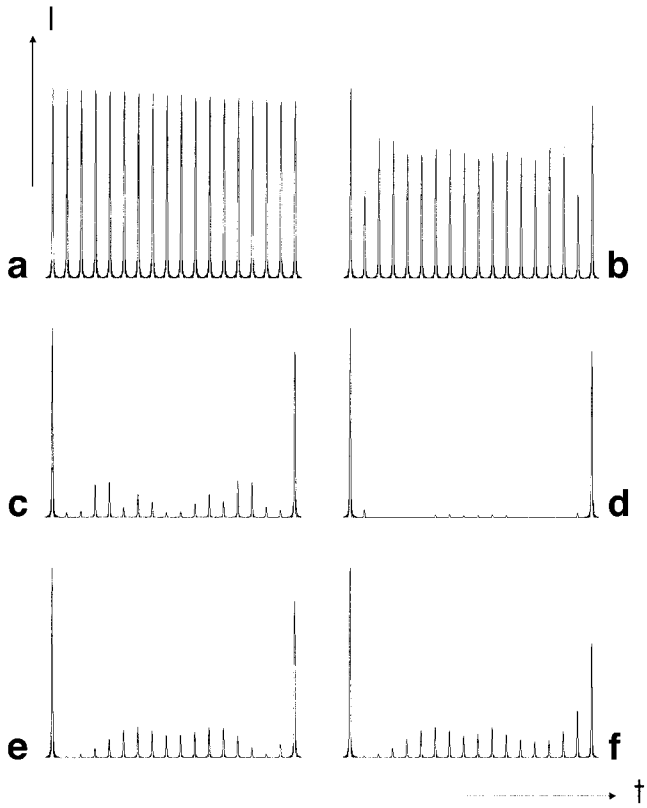

FIG. 4. **a:** Signal intensities of a proper CPMG sequence with 14-ms echo spacing and 18 echoes used as reference. **b–g:** Results of otherwise identical hyperecho sequences. The flip angles and phases of the refocusing pulses are listed in Table 1.

METHODS

All experiments were performed on a 1.5 T system (Magnetom Sonata, Siemens, Germany) equipped with a gradient system with maximum amplitude of 50 mT/m and 200 T/m/s slew rate. Experiments were performed using a TSE sequence with an interecho interval of 14 ms and variable echo train length (ETL). Experiments with variable TE were performed by changing the order of the phase-encoding gradient. For DEFT, a flipback module was appended to the echo train as a time reversal of the excitation part of the sequence such that a flipback pulse was applied to fully refocused magnetization at the exact time of spin-echo refocusing after appropriate rewinding of all gradients.

RESULTS

Basic Signal Behavior

Experimental results illustrating the hyperecho formation are shown in Fig. 4. A CPMG sequence with constant echo spacing of 14 ms was used, and $(2n + 1) = 17$ signals were acquired from a water phantom following an initial 180° refocusing used to generate a full spin-echo for reference of the subsequent echo amplitudes. Only the readout gradient was used. No slice selection was applied in order to maintain homogeneous flip angles over all observed spins. The flip angles and phases of the first 10 pulses are listed in Table 1; all other pulses were calculated according to the symmetry conditions given by Eq. [5]. It is demonstrated that the somewhat counterintuitive recovery of the full signal intensity even after some unusual combinations of refocusing pulses can indeed be realized in practice. For the sequences in Fig. 4c and d identical pulses were used, but in Fig. 4d an additional spoiler gradient was applied orthogonal to the readout gradient to suppress all echoes prior to the hyperecho. Figure 4f illustrates the effect of misadjustment of the central 180° pulse: Just as in normal spin-echo formation, the consequence of refocusing by a pulse with arbitrary flip angle α_r can be regarded as a superposition of an echo train with a 180° refocusing pulse and a signal train with a 0° refocusing pulse (= no pulse). The intensities in each are given by $\sin^2(\alpha_r/2)$ and $\cos^2(\alpha_r/2)$, respectively. The fully refocused part will lead to a hyperecho with amplitude $\sin^2(\alpha_r/2)$. Depending on the choice of α_i, ϕ_i, φ_i of the pulses in the hyperecho train, the $\cos^2(\alpha_r/2)$ part will decay to zero or lead to a small (in general) interference term affecting the phase and amplitude of the hyperecho.

Implementations in RARE Sequences

Figure 5 shows the effect of using hyperechoes in DEFT TSE. Experiments were performed based on sequences with an ETL of 16, TR of 500 ms, and TE of 70 ms. For the conventional sequences used for the images shown in Fig. 5b and c, the refocusing flip angle was set to 90° for all

Table 1
Flip Angles and Phases of the First n Pulses of the Hyperecho Sequences With 2n + 1 Echoes Used for Generating the Signals Shown in Fig. 4

Fig. 4	Flip angles, phases									Ref. pulse
a)	180°, 0°	180°, 0°	180°, 0°	180°, 0°	180°, 0°	180°, 0°	180°, 0°	180°, 0°	180°, 0°	180°, 0°
b)	180°, 0°	90°, 0°	90°, 0°	90°, 0°	90°, 0°	90°, 0°	90°, 0°	90°, 0°	90°, 0°	180°, 0°
c)	180°, 0°	23°, 80°	12°, 70°	77°, 60°	123°, 50°	51°, 40°	34°, 30°	221°, 20°	99°, 10°	180°, 0°
d)	180°, 0°	23°, 80°	12°, 70°	77°, 60°	123°, 50°	51°, 40°	34°, 30°	221°, 20°	99°, 10°	180°, 0°
e)	180°, 0°	10°, 0°	20°, 0°	30°, 0°	40°, 0°	50°, 0°	60°, 0°	70°, 0°	80°, 0°	180°, 0°
f)	180°, 0°	10°, 0°	20°, 0°	30°, 0°	40°, 0°	50°, 0°	60°, 0°	70°, 0°	80°, 0°	120°, 0°
i	1	2	3	4	5	6	7	8	9	10

pulses. For the hyperecho image (Fig. 5a) the first eight refocusing pulses $P_{1..8}(90°, 0°)$ were applied, followed by $P_9(180°, 0°)$, followed by a further eight refocusing pulses $P_{10...17}(-90°, 0°)$. Sixteen echoes were acquired for signal readout and a flipback pulse was applied at the time of the seventeenth echo. Figure 5a and b illustrates the pronounced increase in signal intensity afforded by the flipback mechanism compared to Fig. 5c, in which no flipback was used leading to severe signal saturation. The image using the flipback pulse on the hyperecho (Fig. 5a) shows significantly better retrieval of signals with long T_2, demonstrated by the brighter delineation of CSF-filled spaces.

The use of hyperechoes for increasing the amplitude of the signal carrying the low phase-encoding steps is demonstrated in Fig. 6. The same basic sequence of ETL = 16 (as in Fig. 5) was used, but with a TR/TE of 4000/70 ms. No flipback was used. Variable flip angles were used to establish a smooth transition to the pseudo steady-state amplitude (5,6). For a target refocusing flip angle of 60° the refocusing flip angles were set to 120°, 75°, 65°, 60°, 60°, 60°, 60°, and so on. Compared to the fully refocused image this sequence leads to a reduced image intensity but shows no artifacts, as demonstrated in Fig. 6b. The corresponding hyperecho sequence uses refocusing flip angles 120°, 75°, 65°,180°, 65°, 75°, 120°, 120°, 75°, 65°, 60°, 60°, 60°, and so on, which produces a hyperecho in the seventh refocusing period (TE = 84 ms). A comparison of the resulting image (Fig. 6c) with the reference image (Fig. 6a) reveals the gain in parenchymal signals expected for hyperecho formation in tissues with $T_2 \ll T_1$, whereas CSF appears equally bright. The measured gain in intensity in a ROI in the basal ganglia between the fully refocused image (Fig. 6a) and the hyperecho image (Fig. 6c) was 26%. According to the discussion above (and Fig. 3), this increased intensity reflects the reduced T_2 contrast due to the contribution of stimulated echo pathways. The relative SARs of the low flip angle sequences compared to the fully refocused reference sequence are 13.7% for the low flip angle sequence and 24.4% for the hyperecho sequence.

DISCUSSION

The hyperecho mechanism offers a new degree of freedom for the design of NMR sequences. The ability to rewind the full transverse magnetization after preparation of the spin system with any arbitrary sequence of RF pulses and dephasing steps opens up new possibilities for probing the microenvironment of spins, which could only be hinted at

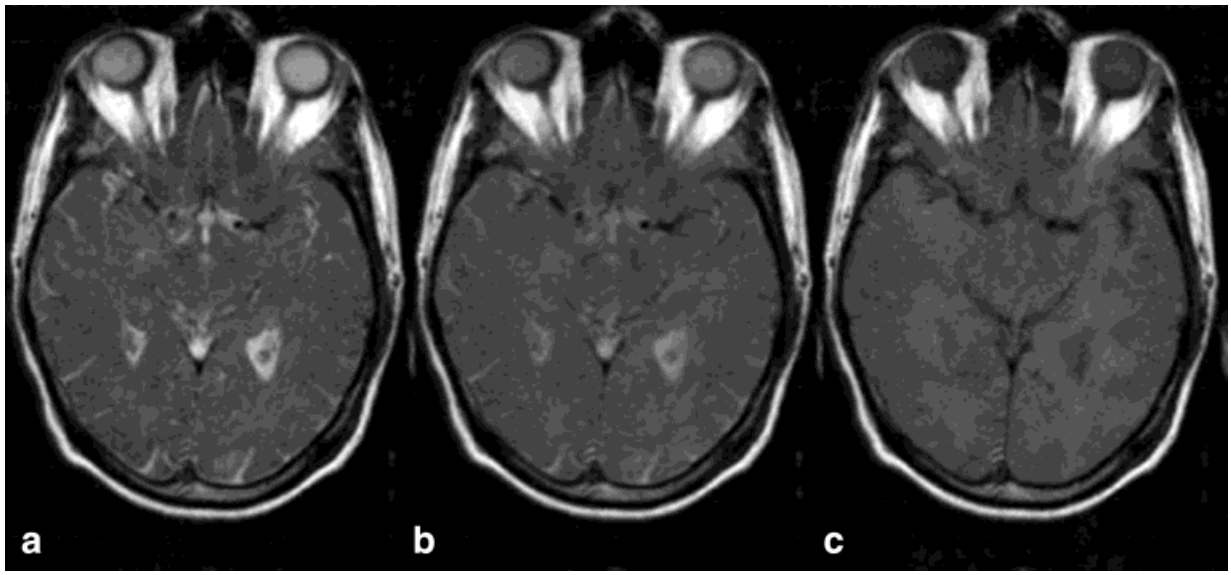

FIG. 5. Images acquired with a DEFT RARE sequence with 90° refocusing flip angles. **a:** The hyperecho mechanism was used to produce a coherent echo for flipback. **b:** A constant refocusing flip angle was used throughout. **c:** An image acquired with parameters identical to those in **b**, but without flipback.

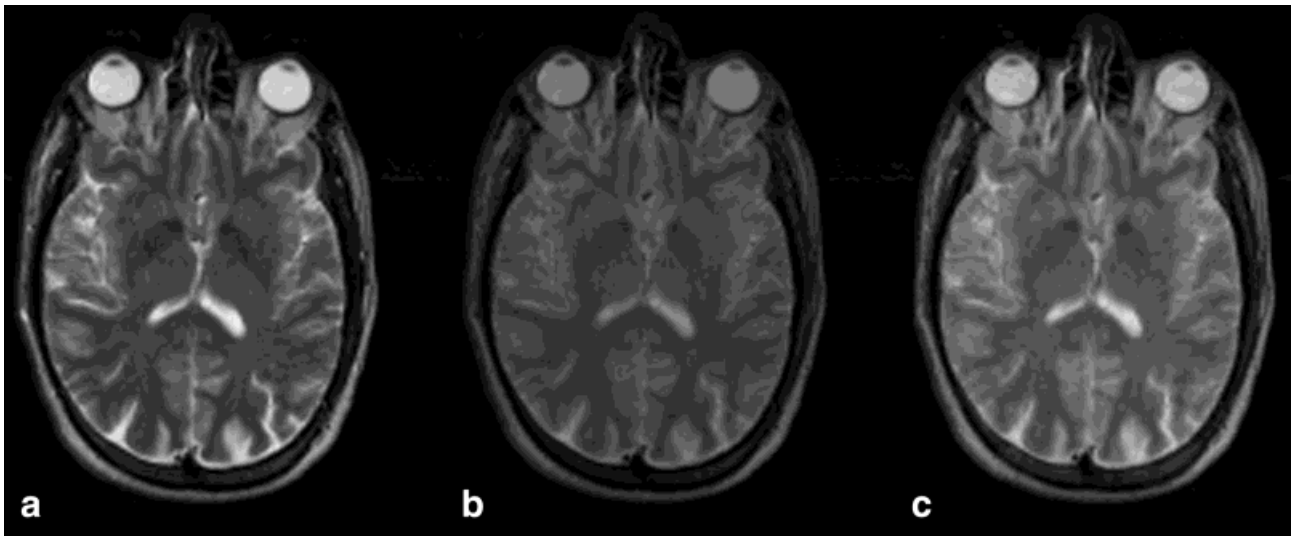

FIG. 6. **a:** A fully refocused TSE image (TR/TE = 4000/84, ETL = 16) compared to **b**, an image acquired with lowered flip angles and **c**, the corresponding hyperecho sequence.

in this first study of the basic mechanism. The hyperecho mechanism, which was pursued originally just for the beauty of reinstalling the coherence of spins after any arbitrary scrambling by a sequence of RF pulses, is already showing some very practical applications, as illustrated in Figs. 5 and 6. It should be noted, however, that these examples were chosen merely to demonstrate basic principles and have not been optimized for practical applications. The effective prolongation of the echo train afforded by the contribution of a stimulated echo mechanism may be especially useful for applications relying on long echo trains. Even at 1.5 T the considerable reduction in SAR will allow the full use of the gradient power to speed up RARE sequences. High-resolution imaging with RF pulse spacings of 3 ms or less may thus become feasible in the near future, even on high-field systems.

It is clear that the hyperecho mechanism offers a very general way to regain dephased signal in arbitrary pulse sequences and is not limited to the RARE sequence. Even gradient-echo sequences may be subject to hyperecho refocusing, as shown in Fig. 7. For better illustration of the hyperecho refocusing conditions, the sequence was set up such that signals from both possible refocusing pathways (10) were generated. It illustrates that the hyperecho from signals S+ will be formed via the S-′-pathways and vice versa (i.e., the central 180° pulse leads to a switch between both possible pathways with respect to hyperecho formation, which has to be taken into account in practical implementations using only one of the two possible signal groups). A more thorough discussion of potential practical applications is beyond the scope of this work.

Furthermore, it should be noted that controlled violation of the hyperecho conditions can be used for selection of subsets of spins. Different refocusing behavior can occur inherently, as in spins in J-coupled multiplets, which will show a different refocusing behavior than uncoupled spins. This also applies for moving spins, in which motion-dependent phase changes will lead to a violation of the hyperecho conditions. Alternatively, one or more modulation intervals $E_S(\varphi_S)$ can be introduced at any time

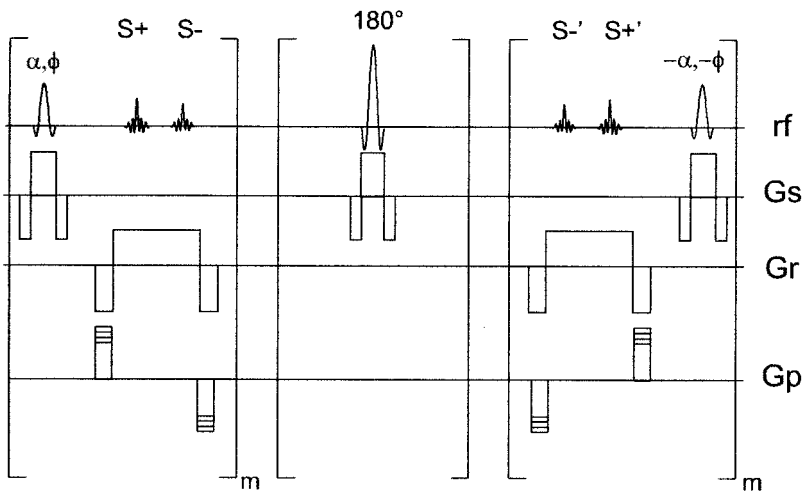

FIG. 7. Basic scheme for using the hyperecho mechanism in a gradient-echo experiment. rf denotes RF pulses and signals; Gs, Gr, and Gp are the slice selection, readout, and phase-encoding gradients, respectively. Gradient echoes are acquired mirror-symmetrically around the central 180° pulse. Gradients are adjusted such that signals from both possible refocusing pathways are generated.

during the hyperecho sequence. The hyperecho conditions will then only be met for spins with $\varphi_S = 0$ (or a multiple of 360°). In the simplest instance, $E_S(\varphi_S)$ can be realized by a mere time interval t_S. In that case, hyperechoes will only be formed for on-resonance spins, whereas off-resonance signals will be attenuated according to the particular choice of α_i, ϕ_i, φ_i. This implementation of hyperechoes can, for example, be used for chemical shift selection analogous to the Dixon technique. The difference lies in the fact that using time shifting in conventional spin echoes will produce fat-water signals with a different phase, while maintaining the amplitude for both species. The hyperecho approach, however, will cause obliteration of the unwanted signals by the proper choice of α_i, ϕ_i, φ_i. Using appropriate gradients in the modulation interval $E_S(\varphi_S)$, other hyperecho sequences can be designed for diffusion encoding, velocity selection, spin tagging, etc. It should be emphasized that adequate obliteration will require carefully designed α_i, ϕ_i, φ_i to ensure sufficient destructive interference of the multiple refocusing pathways.

For some purposes it might be possible to integrate such a spin-selection scheme into the actual acquisition sequence, analogous to the fat suppression technique suggested by Higuchi et al. (11). For more general applications, an appropriate hyperecho selection sequence should be used as a preparation module with subsequent signal readout using echo-planar imaging (EPI), snapshot fast low-angle shot (FLASH) (12), ultra-fast low-angle RARE (U-FLARE) (13), trueFISP, spirals, or any other acquisition technique.

CONCLUSIONS

Hyperechoes offer a new tool for the design of MR sequences. Useful applications have been demonstrated based on RARE sequences. The basic signal formation mechanism suggests other potential uses, the practical applications of which should be demonstrated in further studies.

REFERENCES

1. Hahn EL. Spin echoes. Phys Rev 1950;80:580–594.
2. Hennig J, Nauerth A, Friedburg H. RARE imaging: a fast imaging method for clinical MR. Magn Reson Med 1986;3:823–833.
3. Meiboom S, Gill D. Modified spin-echo method for measuring nuclear relaxation times. Rev Sci Instrum 1958;29:688–691.
4. Hennig J. Multiecho imaging sequences with low refocusing flip angles. J Magn Res 1988;78:397–407.
5. Le Roux P, Hinks RS. Stabilization of echo amplitudes in FSE sequences. Magn Reson Med 1993;30:183–190.
6. Alsop DC. The sensitivity of low flip angle RARE imaging. Magn Reson Med 1997;37:176–184.
7. Hennig J, Scheffler K. Easy improvement of signal-to-noise in RARE sequences with low refocusing flip angles. Magn Reson Med 2000;44: 983–985.
8. van Uijen CM, den Boef JH. Driven-equilibrium radiofrequency pulses in NMR imaging. Magn Reson Med 1984;1:502–507.
9. Busse RF, Riederer SJ, Fletcher JG, Bharucha AE, Brandt KR. Interactive fast spin-echo imaging. Magn Reson Med 2000;44:339–348.
10. Buxton RB. The diffusion sensitivity of fast steady-state free precession imaging. Magn Reson Med 1993;29:235–243.
11. Higuchi N, Hiramatsu K, Mulkern RV. A novel method for fast suppression in RARE sequences. Magn Reson Med 1992;27:107–117.
12. Haase A. Snapshot FLASH MRI. Applications to T1, T2, and chemical-shift imaging. Magn Reson Med 1990;13:77–89.
13. Norris DG. Ultrafast low-angle RARE: U-FLARE. Magn Reson Med 1991;17:539–542.